46th Annual Review of Progress in Quantitative Nondestructive Evaluation
QNDE2019
July 14-19, 2019, Portland, OR, USA

QNDE2019-6765

ULTRASONIC ELASTIC WAVES IN FIBER-METAL LAMINATE STRUCTURES IN PRESENCE OF SOURCES AND DEFECTS

Steffen Tai[1], Ajit Mal
[1]Department of Mechanical and Aerospace Engineering, University of California, Los Angeles

ABSTRACT

Fiber-metal laminate (FML) is a laminated composite combining thin sheets of metal in fiber-reinforced polymer matrix. It has superior properties that are ideal for aerospace applications. To develop the Lamb wave based NDE techniques for FML, numerical simulation to better understand Lamb wave response is important. An efficient framework of coupling the source and the scattering problem is presented to simulate how multiple Lamb modes that are generated by a source is scattered due to a defect. The framework is applied to a titanium-CFRP with a metal-composite interface disbond. The results are compared with those obtained from a dynamic FE method showing very good agreement.

Keywords: Fiber-Metal Laminate, Global Local Method, Lamb Wave, Semi-Analytical Finite Element Method

1. INTRODUCTION

Fiber-metal laminate (FML) is a laminated material consisting of thin layers of metal sheets and fiber layers embedded in an adhesive system. It has advantageous mechanical and physical properties for use as primary load bearing components of aerospace structures [1]. The NDT of FML is necessary due to the complexity of the material system and its vulnerability to the presence of hidden defects. Lamb wave-based damage detection method is potentially an effective and efficient tool for the NDT of FML structures with relatively large areas. Numerical simulation of the complex ultrasonic wave phenomenon is also essential for the development of NDT strategy for FML structures. In previous research, the global-local method (GLM) is used to model the Lamb wave propagation in different structures containing either a source [2] or some defects [3] [4]. This paper presents a framework to model multiple Lamb wave modes generated by a source that interact with a defect. The compute wave field can then be directly compared to the field measurements from experiments. The paper offers important insights into the effects of sources and the scattering characteristics of individual Lamb modes due to different types of defects. The results obtained from the GLM are compared with those obtained from conventional dynamic FE simulations, which shows very good agreement.

2. THE GLOBAL LOCAL FORMULATION

The following analysis considers a large plate subjected to a specified surface traction, representing an ultrasound source transducer, and a defect at some distance away. The GLM uses the finite element method to represent local effects and analytical Lamb modes to represents the far-field solution. Figure 1 illustrates the region in the proximity of the surface load and the region around the defect represented by finite element meshes. Plane strain conditions in the *x-z* plane are assumed.

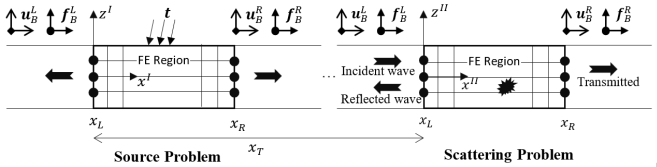

FIGURE 1: ILLUSTRATION OF THE COUPLED SOURCE-SCATTERING PROBLEM WITH GLOBAL-LOCAL METHOD.

The source problem is described under its coordinate system (x^I, z^I) and the scattering problem is described by the coordinate system (x^{II}, z^{II}). The distance between the origins of the two coordinate systems is x_T. The FE region is governed by the discretized form of the equation of motion:

$$\boldsymbol{M\ddot{u} + Ku = f} \tag{1}$$

Assuming harmonic motion of the form $e^{-i\omega t}$, where ω is the circular frequency, equation (1) can be written in frequency domain in terms of the dynamic stiffness matrix $\boldsymbol{D}$ in the form

$$\begin{bmatrix} \boldsymbol{D_{LL}} & \boldsymbol{D_{LI}} & \boldsymbol{D_{LR}} \\ \boldsymbol{D_{IL}} & \boldsymbol{D_{II}} & \boldsymbol{D_{IR}} \\ \boldsymbol{D_{RL}} & \boldsymbol{D_{RI}} & \boldsymbol{D_{RR}} \end{bmatrix} \begin{Bmatrix} \boldsymbol{u_B^L} \\ \boldsymbol{u^I} \\ \boldsymbol{u_B^R} \end{Bmatrix} = \begin{Bmatrix} \boldsymbol{f_B^L} \\ \boldsymbol{f_I} \\ \boldsymbol{f_B^R} \end{Bmatrix} \tag{2}$$

Where $\boldsymbol{D = K - \omega^2 M}$ and the scripts *L, I, R* refers to the left, interior, and right-hand sides of the degrees of freedom (DOFs).

[1] Contact author: steffenwhtai@engineering.ucla.edu

2.1 The Source Problem

For the source problem, equation (2) can be partitioned into left(^{L}), right(^{R}), and interior DOFs that are either free (^{I0}) or subjected to applied traction (^{IF}).

$$\begin{bmatrix} \boldsymbol{D_{LL}} & \boldsymbol{D_{LIF}} & \boldsymbol{D_{LI0}} & \boldsymbol{D_{LR}} \\ \boldsymbol{D_{IFL}} & \boldsymbol{D_{IFIF}} & \boldsymbol{D_{IFI0}} & \boldsymbol{D_{IFR}} \\ \boldsymbol{D_{I0L}} & \boldsymbol{D_{I0IF}} & \boldsymbol{D_{I0I0}} & \boldsymbol{D_{I0R}} \\ \boldsymbol{D_{RL}} & \boldsymbol{D_{RIF}} & \boldsymbol{D_{RI0}} & \boldsymbol{D_{RR}} \end{bmatrix} \begin{Bmatrix} \boldsymbol{u_B^L} \\ \boldsymbol{u^{IF}} \\ \boldsymbol{u^{I0}} \\ \boldsymbol{u_B^R} \end{Bmatrix} = \begin{Bmatrix} \boldsymbol{f_B^L} \\ \boldsymbol{f_{app}} \\ \boldsymbol{0} \\ \boldsymbol{f_B^R} \end{Bmatrix} \quad (3)$$

The applied nodal force f_{app} is the Fourier time transform of the dynamic time dependent nodal force. The displacements and nodal force on either side of the FE boundaries are expressed as a summation of propagating Lamb modes (e.g. A_0, S_0, …) with unknown amplitudes B_n

$$\{\boldsymbol{u_B^L}\} = \left[\overleftarrow{\boldsymbol{Q}}\right]\{\boldsymbol{B_n^L e^{i\overleftarrow{k_n}x_L}}\} \quad (4)$$

$$\{\boldsymbol{f_B^L}\} = -\left[\overleftarrow{\boldsymbol{F}}\right]\{\boldsymbol{B_n^L e^{i\overleftarrow{k_n}x_L}}\} \quad (5)$$

$$\{\boldsymbol{u_B^R}\} = \left[\overrightarrow{\boldsymbol{Q}}\right]\{\boldsymbol{B_n^R e^{i\overrightarrow{k_n}x_R}}\} \quad (6)$$

$$\{\boldsymbol{f_B^R}\} = \left[\overrightarrow{\boldsymbol{F}}\right]\{\boldsymbol{B_n^R e^{i\overrightarrow{k_n}x_R}}\} \quad (7)$$

In equations (4) through (7) the modal displacements and nodal forces are denoted by $[\overleftrightarrow{\boldsymbol{Q}}]$ and $[\overleftrightarrow{\boldsymbol{F}}]$ respectively. The upper arrows indicate the propagation direction with respect to the x direction. The columns of the two matrices correspond to the Lamb modes being considered. The rows are the x and z degrees of freedom on the FE boundary nodes at different z positions and k_n is the wave number for each mode. Nota that, the minus sign on the nodal force expressions is because the negative face normal. For a homogeneous isotropic plate, the modal functions can be found in [5]. For a multilayered composite plate, Waveguide Finite Element Method (WFE) [6] is used to determine the wavenumbers and the modal functions. Solving for B_n from the displacement expressions given in equations (4) and (6) and substituting them into the nodal force expressions given in equation (5) and (7) respectively, the augmented dynamic stiffness matrix is obtained. Then the displacements in the FE region can be solved from the equation

$$\begin{bmatrix} \boldsymbol{D_{LL}} + \left[\overleftarrow{\boldsymbol{F}}\right]\left[\overleftarrow{\boldsymbol{Q}}\right]^{-1} & \boldsymbol{D_{LIF}} & \boldsymbol{D_{LI0}} & \boldsymbol{D_{LR}} \\ \boldsymbol{D_{IFL}} & \boldsymbol{D_{IFIF}} & \boldsymbol{D_{IFI0}} & \boldsymbol{D_{IFR}} \\ \boldsymbol{D_{I0L}} & \boldsymbol{D_{I0IF}} & \boldsymbol{D_{I0I0}} & \boldsymbol{D_{I0R}} \\ \boldsymbol{D_{RL}} & \boldsymbol{D_{RIF}} & \boldsymbol{D_{RI0}} & \boldsymbol{D_{RR}} - \left[\overrightarrow{\boldsymbol{F}}\right]\left[\overrightarrow{\boldsymbol{Q}}\right]^{-1} \end{bmatrix} \begin{Bmatrix} \boldsymbol{u_B^L} \\ \boldsymbol{u^{IF}} \\ \boldsymbol{u^{I0}} \\ \boldsymbol{u_B^R} \end{Bmatrix} = \begin{Bmatrix} \boldsymbol{0} \\ \boldsymbol{f_{app}} \\ \boldsymbol{0} \\ \boldsymbol{0} \end{Bmatrix} \quad (8)$$

2.2 The Coupled Scattering Problem in GLM

The equations for the scattering problem are written in the coordinate system (x^{II}, z^{II}) by omitting the superscript ^{II}.

2.1.1. Left FE Boundary (at $x = x_L = 0$):

The displacements, $\boldsymbol{u_B^L}$ and nodal forces $\boldsymbol{f_B^L}$ at the left boundary nodes would consists of an incident field from the source. Therefore, the incident amplitude coefficient A_{mm} is equal to the right going Lamb mode amplitude coefficients B_n^R of the source problem with a phase change due to the distance x_T between the coordinates in the source problem and the scattering problem. The reflected field has unknown amplitude coefficients $B_n{}^L$ for each mode n:

$$\{\boldsymbol{u_B^L}\} = \left[\overrightarrow{\boldsymbol{Q}}\right]\{\boldsymbol{A_{mm}e^{i\overrightarrow{k_{mm}}(x_L+x_T)}}\} + \left[\overleftarrow{\boldsymbol{Q}}\right]\{\boldsymbol{B_n^L e^{i\overleftarrow{k_n}x_L}}\} \quad (9)$$

$$\{\boldsymbol{f_B^L}\} = -\left[\overrightarrow{\boldsymbol{F}}\right]\{\boldsymbol{A_{mm}e^{i\overrightarrow{k_{mm}}(x_L+x_T)}}\} - \left[\overleftarrow{\boldsymbol{F}}\right]\{\boldsymbol{B_n^L e^{i\overleftarrow{k_n}x_L}}\} \quad (10)$$

Right Hand Side Boundary (at $x = x_R$):

The right-hand displacements and nodal forces at the boundary nodes consist of an incident field from the source problem with phase shift $(x_R + x_T)$, and scattered fields with unknown amplitude coefficients $B_n{}^R$ for each mode n:

$$\{\boldsymbol{u_B^R}\} = \left[\overrightarrow{\boldsymbol{Q}}\right]\{\boldsymbol{A_{mm}e^{i\overrightarrow{k_{mm}}(x_R+x_T)}}\} + \left[\overrightarrow{\boldsymbol{Q}}\right]\{\boldsymbol{B_n^R e^{i\overrightarrow{k_n}x_R}}\} \quad (11)$$

$$\{\boldsymbol{f_B^R}\} = \left[\overrightarrow{\boldsymbol{F}}\right]\{\boldsymbol{A_{mm}e^{i\overrightarrow{k_{mm}}(x_R+x_T)}}\} + \left[\overrightarrow{\boldsymbol{F}}\right]\{\boldsymbol{B_n^R e^{i\overrightarrow{k_n}x_R}}\} \quad (12)$$

It should be noted that the source problem and the scattering problem must have the same wavenumber, then $k_{mm} = k_n$ since their far fields have the same thickness and material properties. Also, it is important to note that the coefficient A_{mm} is taken from the right going amplitude coefficients, B_n^R of the source problem, which is under coordinate x_I, z_I and the phase of A_{mm} (along with $e^{ik_{mm}x_R}$) is expressed in terms of x_I, z_I. This is important when the right-hand scattering coefficient is used. The next step is to use the displacement expression $\{\boldsymbol{u_B^L}\}$ to solve for the unknown amplitude coefficients $\{B_n^L e^{i\overleftarrow{k_n}x_L}\}$ and substitute them into the nodal force expressions $\{\boldsymbol{f_B^L}\}$ to obtain the FE system of equations with the unknown FE region displacements. Using equation (9):

$$\left\{\boldsymbol{B_n^L e^{i\overleftarrow{k_n}x_L}}\right\} = \left[\overleftarrow{\boldsymbol{Q}}\right]^{-1}\{\boldsymbol{u_B^L}\} - \left[\overleftarrow{\boldsymbol{Q}}\right]^{-1}\left[\overrightarrow{\boldsymbol{Q}}\right]\{\boldsymbol{A_{mm}e^{i\overrightarrow{k_{mm}}(x_L+x_T)}}\} \quad (13)$$

Substituting into the left-hand nodal force given in equation (10),

$$\{\boldsymbol{f_B^L}\} = -\left[\overleftarrow{\boldsymbol{F}}\right]\left[\overleftarrow{\boldsymbol{Q}}\right]^{-1}\{\boldsymbol{u_B^L}\} - \left([\overrightarrow{\boldsymbol{F}}] - \left[\overleftarrow{\boldsymbol{F}}\right]\left[\overleftarrow{\boldsymbol{Q}}\right]^{-1}[\overrightarrow{\boldsymbol{Q}}]\right)\{\boldsymbol{A_{mm}e^{i\overrightarrow{k_{mm}}(x_L+x_T)}}\} \quad (14)$$

Similarly, for the right-hand side, solving for amplitude coefficient term from displacement given in equation (11) the nodal forces can be expressed in the form,

$$\{\boldsymbol{f_B^R}\} = \left[\overrightarrow{\boldsymbol{F}}\right]\left[\overrightarrow{\boldsymbol{Q}}\right]^{-1}\{\boldsymbol{u_B^R}\} \quad (15)$$

Substituting the nodal force into equations (2), the final system of equations for displacements in the local region is obtained:

$$\begin{bmatrix} \boldsymbol{D_{LL}} + \left[\overleftarrow{\boldsymbol{F}}\right]\left[\overleftarrow{\boldsymbol{Q}}\right]^{-1} & \boldsymbol{D_{LI}} & \boldsymbol{D_{LR}} \\ \boldsymbol{D_{IL}} & \boldsymbol{D_{II}} & \boldsymbol{D_{IR}} \\ \boldsymbol{D_{RL}} & \boldsymbol{D_{RI}} & \boldsymbol{D_{RR}} - \left[\overrightarrow{\boldsymbol{F}}\right]\left[\overrightarrow{\boldsymbol{Q}}\right]^{-1} \end{bmatrix} \begin{Bmatrix} \boldsymbol{u_B^L} \\ \boldsymbol{u^I} \\ \boldsymbol{u_B^R} \end{Bmatrix} = \begin{Bmatrix} -\left([\overrightarrow{\boldsymbol{F}}] - \left[\overleftarrow{\boldsymbol{F}}\right]\left[\overleftarrow{\boldsymbol{Q}}\right]^{-1}[\overrightarrow{\boldsymbol{Q}}]\right)\{\boldsymbol{A_{mm}e^{i\overrightarrow{k_{mm}}(x_L+x_T)}}\} \\ \boldsymbol{0} \\ \boldsymbol{0} \end{Bmatrix} \quad (16)$$

3. RESULTS AND DISCUSSION

To demonstrate the coupled problem technique, a problem of a titanium-carbon epoxy fiber metal laminate with a disbond is modeled with both global-local method and with conventional

implicit time-stepping FE method in the commercial FE software ABAQUS. Figure 2 shows the FE problem of a uniformly distributed source, 10mm wide with a 5-cycle Hann windowed sinusoidal with 300kHz center frequency, generating Lamb waves that interact with a 10mm long crack 259mm to the right of the center of the source.

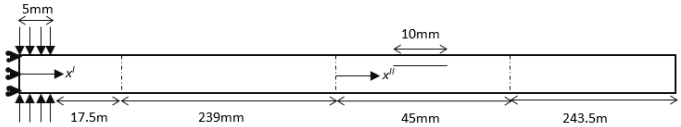

FIGURE 2: SKETCH OF THE SOURCE-DELAMINATION PROBLEM. THE DASHED LINES INDICATE THE FE REGION IN THE GLOBAL LOCAL MODEL.

For the GLM, each "local" region is 45[mm] long which is 25 times the plate thickness. The plate has a stacking sequence of [0/90/Ti/0/90/Ti]s with 12 plies. All plies are 0.15mm thick. The metal plies are titanium and the composite plies are IM7-5250-4 system with the properties as shown in Table 1.

TABLE 1. PROPERTIES USED IN THE FML MODELS. 11 DIRECTION IS ALONG FIBER DIRECTION

	E_{11} [GPa]	E_{33} [GPa]	G_{13} [GPa]	ν_{12}	ν_{23}	Density [kg/m^3]
CFRP	162.0	9.685	5.861	0.318	0.402	1578
Ti	100.0			0.330		4760

Note that for conventional FE approach, only the right half of the problem is modeled with the use of symmetric boundary conditions. The model has a total length of 550[mm] in *x*-direction. A "crack seam" which allows the separation of nodes is created to represent the disbond between the first 90/Ti interface in the upper half of the laminate. The debonded face is traction free. The time stepping FE model has a total simulation period of 0.175[ms] using 800 time-steps (with step time of 2.1875e^{-4}[ms]). Figure 3 shows the results from the conventional FE and global-local method for the vertical displacement 20mm to the right of the source due solely to S_0 mode. The reflection after 0.1ms from the disbond in the ABAQUS solution is part of the scattering solution and therefore is not plotted here.

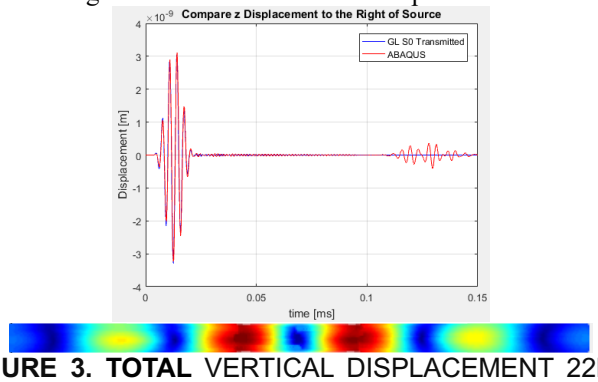

FIGURE 3. TOTAL VERTICAL DISPLACEMENT 22MM TO THE RIGHT OF THE SOURCE FROM GL AND FE SOLUTION, AND DISPLACMENT FIELD NEAR THE SOURCE AT 6.7 MIRCO SECOND.

Figure 4, shows the comparison between of the FE and global-local solution to the left of the disbond.

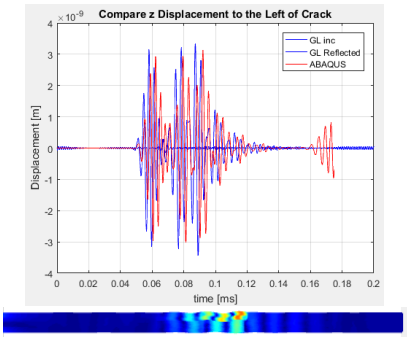

FIGURE 4. TOTAL VERTICAL DISPLACEMENT 17.5MM TO THE LEFT OF THE DISBOND'S LEADING EDGE

Both the ABAQUS and GL solutions predict that the reflected waveform has two packets due to the leading and trailing edges of the disbond, which is visualized in the contour plot of the displacement field.

4. CONCLUSIONS

This research demonstrates a framework that couple the source and the scattering problem to model a physical phenomenon. This method, when using WFE, has the ability to model multilayered composites such as FML for different types of defects. The solution is compared with the dynamic FE result. Both solutions show that the S_0 mode is generated from the applied load and the reflected waves consist of two packets from the leading and trailing edges of the disbond.

ACKNOWLEDGEMENTS

This research is funded by the Aerospace Corporation (Contract #: 20182871).

REFERENCES

[1] R. C. Alderliesten and R. Benedictus, "Fiber/Metal Composite Technology for Future Primary Aircraft Structures," *Journal of Aircraft,* vol. 45, no. 4, pp. 1182-1189, 2008.

[2] C. Schaal, R. M'Closkey and A. Mal, "A Semi-analytical Method for Caculating Resonator Energy Loss into Plate Substrates," *IEEE International Symposium on Inertial Sensors and Systems,* pp. 17-20, 2016.

[3] Y. N. Al-Nassar, S. K. Datta and A. H. Shah, "Scattering of Lamb Waves by a Normal Rectangular Strip Weldment," *Ultrasonics,* vol. 29, no. March, pp. 125-132, 1991.

[4] Z. Chang and A. Mal, "Scattering of Lamb Waves from a Rivet Hole with Edge Cracks," *Mechanics of Materials,* vol. 31, pp. 197-204, 1999.

[5] C. Schaal, H. Samajder, H. Baid and A. Mal, "Rayleigh to Lamb Wave Conversion at a Delamination-like Crack," *Journal of Sound and Vibration,* vol. 353, pp. 150-163, 2015.

[6] M. Maess, J. Herrmann and L. Gaul, "Finite Element Analysis of Guided Waves in Fluid-Filled Corrugated Pipes," *Journal of Acoustic Society,* vol. 121, no. 3, pp. 1313-1323, 2007.